

See discussions, stats, and author profiles for this publication at: <https://www.researchgate.net/publication/342493237>

Brain Graph Super-Resolution for Boosting Neurological Disorder Diagnosis using Unsupervised Multi-Topology Connectional Brain Template Learning

Article in *Medical Image Analysis* · October 2020

DOI: 10.1016/j.media.2020.101768

CITATIONS

12

READS

514

4 authors:



Islem Mhiri

Université Clermont Auvergne

10 PUBLICATIONS 51 CITATIONS

[SEE PROFILE](#)



Anouar Ben Khalifa

University of Sousse

51 PUBLICATIONS 472 CITATIONS

[SEE PROFILE](#)



Mohamed Ali Mahjoub

University of Sousse

163 PUBLICATIONS 982 CITATIONS

[SEE PROFILE](#)



Islem Rekik

Istanbul Technical University

188 PUBLICATIONS 1,563 CITATIONS

[SEE PROFILE](#)

Some of the authors of this publication are also working on these related projects:



Knowledge extraction [View project](#)



Automatic Speech Emotion Recognition [View project](#)

Brain Graph Super-Resolution for Boosting Neurological Disorder Diagnosis using Unsupervised Multi-Topology Connectional Brain Template Learning

Islem Mhiri^{a,b}, Anouar Ben Khalifa^b, Mohamed Ali Mahjoub^b, Islem Rekik^{a,c,*}

^a*BASIRA lab, Faculty of Computer and Informatics, Istanbul Technical University,
Istanbul, Turkey*

^b*Université de Sousse, Ecole Nationale d'Ingénieurs de Sousse, LATIS- Laboratory of
Advanced Technology and Intelligent Systems, 4023, Sousse, Tunisie;*

^c*School of Science and Engineering, Computing, University of Dundee, UK*

Abstract

Existing graph analysis techniques generally focus on *decreasing* the dimensionality of graph data (i.e., removing nodes, edges, or both) in diverse predictive learning tasks in pattern recognition, computer vision, and medical data analysis such as dimensionality reduction, filtering and embedding techniques. However, ***graph super-resolution*** is strikingly lacking, i.e., the concept of *super-resolving* low-resolution (LR) graphs with n_r nodes into high-resolution graphs (HR) with $n_{r'} > n_r$ nodes. Particularly, learning how to automatically generate HR brain connectomes, without resorting to the computationally expensive MRI processing steps such as image registration and parcellation, remains unexplored. To fill this gap, we propose the first technique to super-resolve undirected fully connected graphs with application to brain connectomes. *First*, we root our brain graph super-resolution (BGSR) framework in learning how to estimate a centered LR population-based brain graph representation, coined as connectional brain template (CBT), acting as a proxy in the target BGSR task. Specifically, we hypothesize that the estimation of a well-representative and centered CBT would help better capture the *individuality* of each LR brain graph via its residual distance from the population-based CBT. This will eventually al-

*Corresponding author; Dr Islem Rekik, <http://basira-lab.com/>, GitHub code:
<https://github.com/basiralab/BGSR>

low an accurate identification of the most similar individual graphs to a new testing graph in the LR domain for the target prediction task. *Second*, we leverage the estimated LR CBT (i.e., population mean) to derive residual LR brain graphs, capturing the deviation of all subjects from the estimated CBT. *Third*, we learn multi-topology LR graph manifolds using different graph topological measurements (e.g., degree, closeness, betweenness) by estimating residual LR similarity matrices modeling the relationship between pairs of residual LR graphs. These are then fused so we can effectively identify for each testing LR subject its most K similar training LR graphs. *Last*, the missing testing HR graph is predicted by averaging the HR graphs of the K selected training subjects. Predicted HR from LR functional brain graphs boosted classification results for autistic subjects by 16.48% compared with LR functional graphs.

Keywords: graph super-resolution, brain connectomes, connectional brain template learning, topology-based residual graph manifold learning, neurological disorder diagnosis, brain graph fusion

1. Introduction

Graph analysis techniques are very popular in different research fields including pattern recognition (Bunke and Riesen, 2011), computer vision (Xiao et al., 2013) and medical data analysis (Kruschwitz et al., 2015; Mijalkov et al., 2017; Bassett et al., 2017; Oxtoby et al., 2017; Chen and Pan, 2018). Thanks to their ability to model easily complex relationships between data samples and features (Hegeman and Iosup, 2018), a large number of these techniques focus on decreasing the dimensionality of graph data (i.e., removing nodes, edges, or both) including dimensionality reduction Shen et al. (2017), filtering (Chen et al., 2014) and embedding techniques (Goyal and Ferrara, 2018). To name a few, (Yan et al., 2007) proposed a dimensionality reduction technique, namely marginal Fisher analysis, based on graph embedding. Another work (Huang and Huang, 2018) applied a filtering approach based on removing nodes and edges in order to reduce the size of a large graph. Surprisingly, *graph super-resolution* remains an unexplored topic which might help solve several research problems, particularly in medical data analysis for neurological disorder diagnosis. On the other hand, *image super-resolution* has seen a surge of interest in image processing field (Park et al., 2003). It can offer solutions to remove the degradations caused

by the imaging process for facilitating better scene recognition and content visualization (Tian and Ma, 2011). For instance, (Bahrami et al., 2017b) recently proposed a machine-learning based method to predict 7T-like magnetic resonance images (MRI) from low-resolution 3T MRI, thereby producing MR images of the brain with better tissue contrast and higher resolution than the conventional 3T MRI while circumventing the scarcity of 7T scanners worldwide.

While a few image super-resolution techniques have been proposed for MRI super-resolution (Bahrami et al., 2016, 2017b,a), graph super-resolution techniques are currently absent. Typically, in medical image analysis, to generate brain graphs at different resolutions, one needs to first pre-process the MRI data including skull stripping, brain extraction, registration to a brain atlas (i.e., brain template) for parcellating the brain into n_r anatomical regions of interest (ROIs) (Glasser et al., 2016; Makropoulos et al., 2018; Bastiani et al., 2019). A typical brain graph or connectome is composed of n_r nodes, where each node represents an ROI and the strength of the edge connecting two ROIs models their relationship (e.g., correlation in neural firing). This process has two severe limitations: (1) it is very time consuming (it can last up to a few hours when using refined deformable registration), and (2) it is sensitive to the deployed pre-processing methods including registration, atlas-to-image label propagation, which might preclude the comparison of healthy and disordered brain connectomes produced using different MRI pre-processing pipelines. In fact, parcellation methods use predefined coarsely parcellated brain atlases such as Automated Anatomical Labelling (AAL) with 90 ROIs, which define the size or *resolution* of the resulting brain connectomes (Bellec et al., 2015). For instance, the commonly used statistical parametric mapping (SPM) software (Ashburner, 2012) for generating functional connectomes performs automated anatomical parcellation of brain MR images. FreeSurfer was also utilized for generating morphological connectomes (Mahjoub et al., 2018). It also performs automated labeling and allows to register cortical surfaces to Desikan-Killiany surface template (Li et al., 2013). However, its computational time can go up to 20h per subject to run the complete image processing pipeline (Li et al., 2013), eventually producing hemispheric surface parcellation. *Ideally, given a low-resolution brain graph, one would learn how to synthesize brain graphs automatically at higher resolutions while circumventing the use of time-consuming image processing pipelines.*

To this aim, we propose the first learning-based technique to superresolve

undirected fully connected graphs with application to brain connectomes with the aim of boosting the diagnosis of neurological disorders (e.g., autism spectrum disorder (ASD)). Inspired from fundamental works on predicting spatiotemporal (Rekik et al., 2015, 2016; Ezzine and Rekik, 2019) and multi-view (Zhu and Rekik, 2018; Bessadok et al., 2019) brain data from a baseline observation, we formalize brain graph super-resolution (BGSR) as a prediction task: predicting high-resolution graphs from low-resolution graphs. Remarkably, all these predictive works are based on the following assumption: if one can learn how to identify the most similar training samples to the testing sample in the source domain, one can predict the target testing sample in the target domain by fusing the selected target training samples. In this context, the source domain denotes the domain where low-resolution data points live and the target domain as domain where the high-resolution data points to predict are nested. In this work we adopt another variant of this hypothesis as illustrated in **Fig. 1**. Given a representative and centered training LR population-driven brain graph, *the deviation of each sample from the center (i.e., residual)* better captures the individual traits of each sample, and in turn, better characterizes the similarity between each training and testing LR brain graph. Therefore, by identifying the most similar training residuals to the testing residual in the low-resolution domain, we can better predict the target testing sample in the high-resolution domain by averaging the selected training subjects (**Fig. 1**).

The proposed BGSR framework comprises several steps. *First*, we root our brain graph super-resolution (BGSR) framework in learning how to estimate a centered LR population-based brain graph, namely a connectional brain template (CBT), acting as a proxy in the target BGSR task. Particularly, we hypothesize that the estimation of a well-representative and centered CBT would help better capture the *individuality* of each LR brain graph via its residual distance from the population-based CBT. This will ultimately allow an accurate identification of the most similar individual graphs to a new testing graph in the LR domain for the target prediction task. *Second*, we leverage the estimated LR CBT (i.e., population mean) to derive residual LR brain graphs, capturing the deviation of all subjects from the estimated CBT. *Third*, we learn multi-topology LR graph manifolds using different graph topological measurements (e.g., degree, closeness, betweenness), where we learn residual LR similarity matrices modeling the relationship between pairs of training and testing residual LR graphs. These are then fused so we can effectively identify for each testing LR subject its most K similar

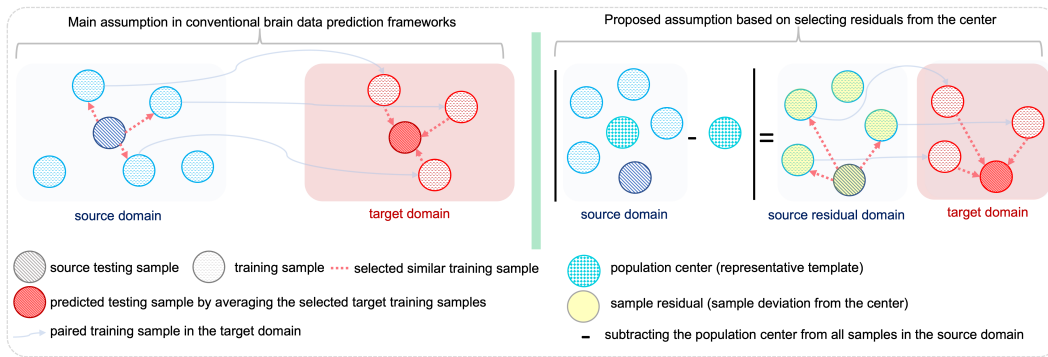


Figure 1: *Proposed brain graph super-resolution assumption for predicting high-resolution brain graphs (target domain) from low-resolution brain graphs (source domain.)* (**Left panel**) In this illustration, we sketch the assumption adopted in several brain data predictive works stating that: if one can learn how to identify the most similar training samples to the testing sample in the source domain, one can predict the target testing sample in the target domain by fusing the selected target training samples. (**Right panel**) In this paper, we root our framework in the following assumption: Given a representative center sample of the training sample population in the source domain, the deviation of each sample (i.e., residual) from the population center better captures the individual traits of each sample, and in turn, better characterizes the similarity between each training sample and testing sample in the source domain. Hence, by identifying the most similar training residuals to the testing residual in the low-resolution domain, we can better predict the target testing sample in the high-resolution domain by averaging the selected training samples in the target domain.

training LR graphs. *Last*, we predict the testing HR graph by averaging the HR graphs of the K selected training subjects. The main contributions of our method are four-fold:

1. *On a conceptual level*, we propose the first graph super-resolution technique with the aim of boosting neurological disorder diagnosis.
2. *On a methodological level*, we present a novel formalization of data super-resolution rooted in using deviations (i.e., residual measurements) from a population center that we learn to eventually better capture similarities between data points. Specifically, we propose to use topological measures of the residual networks to learn a multi-topology residual manifold that better captures the similarities between pairs of samples (networks).
3. *On a computational level*, our method reconstructs HR graphs without resorting to any computationally demanding MRI processing step such as non-rigid registration and parcellation. We directly learn how to *predict a high-resolution graph from a low-resolution graph*.
4. *On a generic level*, our framework is a generic method as it can be applied to brain networks derived from any neuroimaging modality (e.g., morphological and structural connectomes) given that they are isomorphic.

2. Proposed framework

Fig. 2 provides an overview of the key steps of our proposed brain graph super-resolution (BGSR) using unsupervised multi-topology connectional brain template learning. In the first stage, we learn how to estimate a centered LR population-driven brain graph for HR brain graphs prediction. To this aim, we first downsample each HR brain graph to produce a LR brain graph. Next, we estimate a representative and centered CBT by learning multiple cluster-specific CBTs in the low-resolution domain, each occupying the center of a cluster of brain graphs. To tease apart the different clusters, thereby capturing the heterogeneous distribution of the data, we leverage Multi Kernel Manifold Learning (MKML) framework ([Wang et al., 2018](#)). MKML effectively learns sample-to-sample similarity measures that best fit the structure of the data by combining multiple kernels. Next, the learned similarity matrix is used to cluster the LR brain graphs into different subpopulations. We then estimate the cluster-specific CBT by using similarity network fusion (SNF) technique ([Wang et al., 2014a; Rekik et al., 2017](#)). SNF integrates the

LR brain graphs into a single brain graph, in a non-linear way, using both local and global diffusion processes. SNF is one of the most effective graph fusion techniques as it is able to (i) capture both common patterns and complementary information across samples, (ii) derive useful information even from a small number of samples, (iii) handle noise and data heterogeneity, and (iv) scale to a large number of features. To estimate the final CBT, we apply SNF to fuse all cluster-specific CBT estimated for each subpopulation. The last step in this stage is to define the residual LR brain graphs by computing the absolute difference between the estimated CBT and each LR brain graphs, capturing the deviation of each individual subject from the population mean (or center).

In the second stage, we use diverse graph topological measurements (e.g., degree centrality, closeness centrality and betweenness centrality) to learn multi-topology LR graph manifolds. In fact, these centrality metrics allow to identify the most significant ROIs (central nodes) in information flow in brain graphs (Joyce et al., 2010). (Freeman, 1978) showed that degree, betweenness and closeness are three cardinal aspects of topological centrality. Hence, we adopt these metrics in order to characterize both local and global relationships between brain ROIs. Next, we non-linearly fuse the learned LR manifold similarity matrices to identify the K most similar LR training samples in topological properties to the target. By simply retrieving and averaging their corresponding K graphs in the high-resolution domain, we predict the testing HR brain graph (**Fig. 1**).

2.1. Low-resolution brain graph generation and feature extraction

In this section, we aim to create low-resolution brain graphs which represent the source domain in our work. Throughout the paper, matrices are denoted by boldface capital letters, e.g., \mathbf{X} , vectors by boldface lowercase letters, e.g., \mathbf{x} , and scalars are denoted by lowercase letters, e.g., x . \mathbf{X}^T denotes the transpose operator. For easy reference, we have summarized the major mathematical notations in (**Table 1**).

Several image-based super-resolution works resort to downsampling high-resolution images to train and evaluate their models, which degrades the quality of the input data. For instance, (Wang et al., 2014b) applied a downsampling method to obtain LR images of size 256×256 and 128×128 from 512×512 HR images. Also, (Rueda et al., 2013) downsampled HR images to create LR images and learn the mapping from an LR image to an HR image using multi-resolution dictionary learning. In another work,

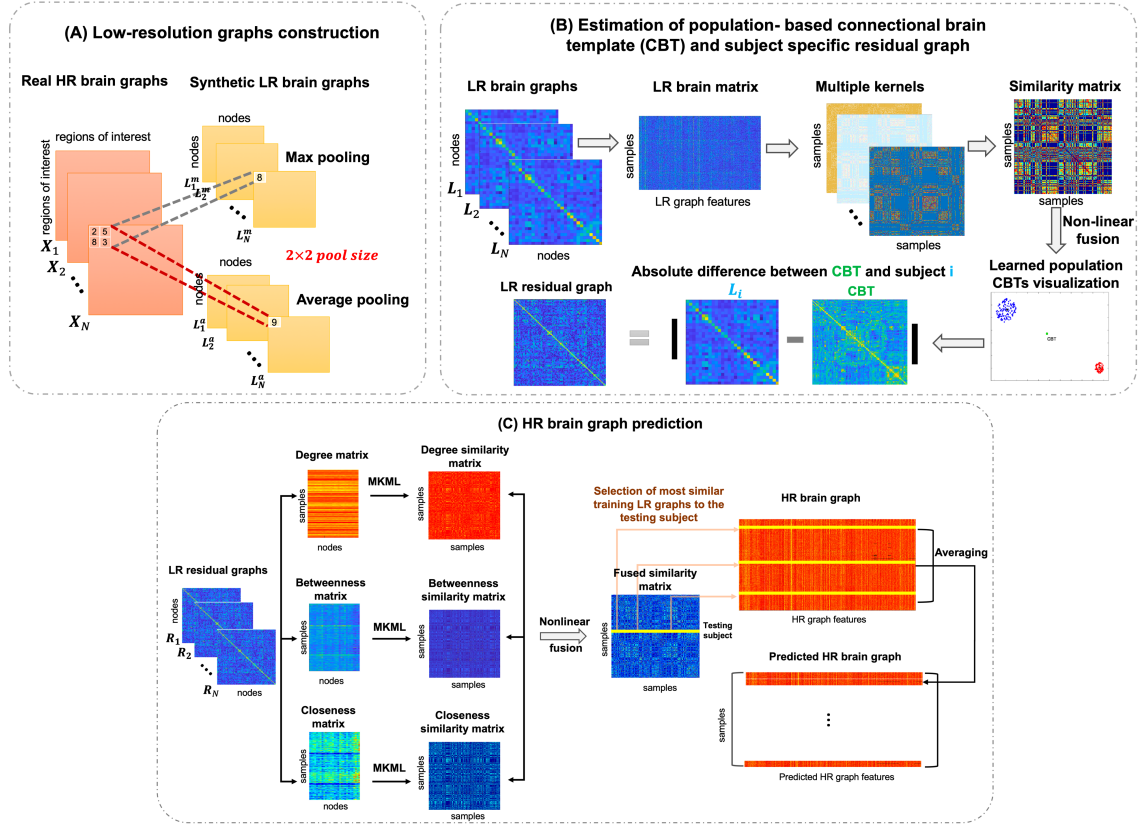


Figure 2: Illustration of the proposed brain graph super-resolution (BGSR) with application to functional brain connectomes. **(A)** Synthetic LR brain graphs construction by downsampling high-resolution brain graphs using max pooling and average pooling. **(B)** In order to disentangle the heterogeneous distribution of LR brain graphs, we adapt multi kernel manifold learning (MKML) (Wang et al., 2018) to first cluster LR graphs into different homogeneous clusters. For each cluster, a local centered CBT estimated using similarity network fusion (SNF (Wang et al., 2014a)), then we merge all these local cluster-specific CBTs into a global population-centered CBT. Next, we compute the absolute difference between each LR brain graph and CBT to create residual graphs for training and testing samples. **(C)** For each *residual* brain graph, we compute three topological measurements (betweenness, closeness and degree), then we unsupervisedly learn a similarity matrix associated with each LR topological manifold. Next, we non-linearly fuse the three similarity matrices into a single matrix, which is used to identify the most similar K training subjects to the testing subject in the LR domain. Last, we average the HR graphs of the K selected training subjects to predict the testing HR graph in the target domain.

Table 1: Major mathematical notations used in this paper.

Mathematical notation	Definition
N	total number of brain graphs
n_r	number of anatomical regions of interest at high resolution
$n_{r'}$	number of anatomical regions of interest at low resolution
\mathbf{X}_i	HR brain graph in $\mathbb{R}^{n_r \times n_r}$ of the i -th subject
\mathbf{L}_i	LR brain graph in $\mathbb{R}^{n_{r'} \times n_{r'}}$ of the i -th subject
\mathbf{R}_i	LR residual brain graph in $\mathbb{R}^{n_{r'} \times n_{r'}}$ of the i -th subject
\mathbf{c}_i	feature vector of a subject i
\mathbf{k}_k	k -th learning kernel in $\mathbb{R}^{N \times N}$
\mathbf{S}	similarity matrix in $\mathbb{R}^{N \times N}$
N_{nc}	number of samples in the n_c^{th} cluster
N_c	number of clusters
n_k	number of kernels
\mathbf{w}_k	weighting vector of the kernels in \mathbb{R}^{n_k}
\mathbf{L}	latent matrix in $\mathbb{R}^{N \times N_c}$
\mathbf{I}_N	identity matrix in $\mathbb{R}^{N \times N}$
$\mathbf{G}_i = (\mathbf{V}_i, \mathbf{E}_i)$	brain network graph of a single subject
\mathbf{V}_i	brain ROIs (nodes)
\mathbf{E}_i	edges connecting brain regions
\mathbf{Q}_i	kernel similarity matrix of the i -th subject
\mathbf{W}_i	connectivity matrix of the i -th subject
\mathbf{P}_i	full kernel matrix of the i -th subject
CBT_c	LR cluster-specific CBT in $\mathbb{R}^{n_{r'} \times n_{r'}}$
CBT	LR CBT in $\mathbb{R}^{n_{r'} \times n_{r'}}$
f_n	number of selected features
\mathbf{D}	LR degree centrality matrix in $\mathbb{R}^{N \times n_{r'}}$
\mathbf{C}	LR closeness centrality matrix in $\mathbb{R}^{N \times n_{r'}}$
\mathbf{B}	LR betweenness centrality matrix in $\mathbb{R}^{N \times n_{r'}}$

(Bahrami et al., 2017b) downsampled all 7T MR images with a factor of 3 to reduce the quality of 7T MR images to evaluate the proposed 7T MRI super-resolution technique. By doing so, downsampling decreases the number of voxels and also causes the loss of image details.

In this paper, we also adopt a similar strategy to train and evaluate our BGSR technique by downsampling high-resolution brain graphs. Specifically, given a population of N HR brain graphs, each graph i is encoded in a matrix \mathbf{X}_i of size $n_r \times n_r$, where n_r denotes the number of ROIs. To synthesize LR brain graphs, we downsample each HR brain graph using two different approaches: non-linear max pooling and linear average pooling (Fig. 2–A). Particularly, We run 2×2 filter over \mathbf{X}_i where each 2×2 group of connectivity weights in \mathbf{X}_i is reduced to a single weight by selecting the maximum weight for max pooling and averaging for average pooling. Both approaches produce LR brain graphs of size $n_{r'} \times n_{r'}$, where $n_{r'} = \frac{n_r}{4}$. Since each matrix \mathbf{L}_i is symmetric, we vectorize the upper off-diagonal triangular part to define a connectivity feature vector \mathbf{c}_i for subject i , then concatenate

them all together into a functional data matrix of size $N \times \frac{n_{r'} \times (n_{r'} - 1)}{2}$. In the next step, we learn how to estimate a population-driven low-resolution CBT for super-resolving LR brain graphs.

2.2. Population-based connectional brain template (CBT) learning

In a first stage, given a set of N LR brain graphs, we aim at estimating a centered and representative connectional brain template for HR brain graph synthesis. In the first step, we aim to disentangle the heterogeneous distribution of the LR graphs by leveraging multiple kernels to learn a connectomic manifold. Thus, we adopt the recently developed method multi kernel manifold learning (MKML) proposed in (Wang et al., 2017). In the second step, we iteratively diffuse and fuse brain graphs lying on the same manifold, thereby estimating a cluster-specific CBT. Last, we average all cluster-specific CBTs into a whole population-centered CBT. In what follows, we will detail each of these steps for the proposed CBT estimation.

(i) **CBT-based multi-kernel manifold learning (MKML).** We first cluster similar LR graphs into subspaces using multiple kernel learning (Wang et al., 2017). Specifically, we learn a LR graph-based manifold by estimating the weights $\{w_k\}_{k=1}^{n_k}$ associated with a set of n_k Gaussian kernels $\{\mathbf{K}_k\}_{k=1}^{n_k}$ with different bandwidths that can capture heterogeneous LR data distributions. We represent each graph by a feature vector extracted from the upper triangular part of its adjacency matrix as it is symmetric.

Each Gaussian kernel is defined as: $\mathbf{K}(\mathbf{c}^i, \mathbf{c}^j) = \frac{1}{\epsilon_{ij}\sqrt{2\pi}} e^{-\frac{|\mathbf{c}^i - \mathbf{c}^j|^2}{2\epsilon_{ij}^2}}$.

where \mathbf{c}^i and \mathbf{c}^j denote the feature vectors of the i -th and j -th graphs, respectively. ϵ_{ij} is defined as: $\epsilon_{ij} = \sigma(\mu_i + \mu_j)/2$, where σ is a tuning parameter and $\mu_i = \frac{\sum_{l \in KNN(\mathbf{c}^i)} |\mathbf{c}^i - \mathbf{c}^l|}{k}$, where $KNN(\mathbf{c}^i)$ represents the top k neighboring subjects of subject i .

The weighted kernels are then averaged to produce the target similarity matrix \mathbf{S} . These are estimated along with an $N \times N_c$ latent matrix \mathbf{L} capturing N_c (number of clusters) inherent subspaces where our LR graphs lie by solving the following optimization problem:

$$\min_{\mathbf{S}, \mathbf{L}, \mathbf{w}} \sum_{i,j,k} -w_k \mathbf{K}_k(\mathbf{c}^i, \mathbf{c}^j) \mathbf{S}_{ij} + \beta \|\mathbf{S}\|_F^2 + \eta \text{tr}(\mathbf{L}^T (\mathbf{I}_N - \mathbf{S}) \mathbf{L}) + \rho \sum_k w_k \log w_k \quad (1)$$

Subject to: $\sum_k w_k = 1$, $w_k \geq 0$, $\mathbf{L}^T \mathbf{L} = \mathbf{I}_{N_c}$, $\sum_j \mathbf{S}_{ij} = 1$, and $\mathbf{S}_{ij} \geq 0$ for all (i, j) .

The first term refers to the relation between the similarity and the kernel distance with weights w_l between two graphs. The second term denotes a regularization term that avoids over-fitting the model to the data. Therefore, the third term along with the constraint on \mathbf{L} enforces the low-rank structure of the learned similarity \mathbf{S} which should be small if the distance between a pair of graphs is large. The matrix $(\mathbf{I}_N - \mathbf{S})$ denotes the graph Laplacian (Von Luxburg, 2007), where \mathbf{I}_N is the identity matrix, and the trace-minimization problem enforces approximately N_c connected components in a similarity graph that consists of nodes representing the cells and edge weights corresponding to pairwise similarity values in \mathbf{S} . The last term imposes constraints on the kernel weights to avoid selection of a single kernel. An alternating convex optimization is adopted where each variable is optimized while fixing the other variables until convergence (Wang et al., 2017). Once the similarity matrix \mathbf{S} is learned, we perform subpopulation identification by extracting the N_c blocks where similar LR brain graphs group together.

(ii) Cluster-specific CBT estimation using non-linear brain graph diffusion. The basic idea of our CBT estimation lies in first estimating cluster-specific CBTs for disentangling LR brain graph data heterogeneity, then fusing all the cluster-specific CBTs to produce a global presentative center of all individuals in the population (Fig. 2–B). For each individual graph i in the n_c^{th} subpopulation (or cluster) composed of N_{n_c} graphs, where N_{n_c} denotes the cardinal of the n_c^{th} cluster, we define a graph $\mathbf{G}_i(\mathbf{V}_i, \mathbf{E}_i)$ where each vertex in \mathbf{V}_i denotes an ROI and each edge in \mathbf{E}_i connecting two ROIs k and l denotes the strength of their connectivity. Prior to applying similarity network fusion (SNF) method (Wang et al., 2014a), we first normalize each feature vector \mathbf{c} as follows: $\tilde{\mathbf{c}} = \frac{\mathbf{c} - \mathbf{E}(\mathbf{c})}{\sqrt{var(\mathbf{c})}}$, where $\tilde{\mathbf{c}}$ denotes the corresponding normalized feature vector. $\mathbf{E}(\mathbf{c})$ denotes the empirical mean of \mathbf{c} and $var(\mathbf{c})$ represents the variance of \mathbf{c} . Next, we define a kernel similarity matrix \mathbf{Q}_i for each individual LR graph i in the population, which encodes its local structure by computing the similarity between each of its elements ROI k and its nearest ROIs l as follows:

$$\mathbf{Q}_i(k, l) = \begin{cases} \frac{\mathbf{W}_i(k, l)}{\sum_{p \in N_k} \mathbf{W}_i(k, p)} & l \in N_k \\ 0, & otherwise \end{cases} \quad (2)$$

where N_k deotes the set of q neighbors of ROI k identified using KNN

algorithm.

\mathbf{W}_i represents the connectivity matrix where element $\mathbf{W}_i(k, l)$ denotes the connectivity between ROIs k and l for graph i .

In the network cross-diffusion process, one needs to define a status matrix, also referred to as the global topology matrix \mathbf{P}_i , capturing the global structure of each individual i and carrying the full information about the similarity of each ROI to all other ROIs as follows:

$$\mathbf{P}_i(k, l) = \begin{cases} \frac{\mathbf{W}_i(k, l)}{2\sum_{p \neq k} \mathbf{W}_i(k, p)} & l \neq k \\ 1/2, & l = k \end{cases} \quad (3)$$

We notice that SNF is robust to noise thanks to \mathbf{Q} , which can reduce noise between instances. In order to integrate the different networks into a single network, the status matrices \mathbf{P}_i are iteratively updated for each individual connectome by diffusing the the global structure \mathbf{P}_j of $N_{n_c} - 1$ networks ($j \neq i$) along the local structure \mathbf{Q}_i of subject i as follows:

$$\mathbf{P}_i = \mathbf{Q}_i \times \left(\frac{\sum_{j \neq i} \mathbf{P}_j}{N_{n_c} - 1} \right) \times \mathbf{Q}_i^T, \quad j \in \{1, \dots, N_{n_c}\} \quad (4)$$

where $\frac{\sum_{j \neq i} \mathbf{P}_j}{N_{n_c} - 1}$ denotes the diffusion structure computed as the mean global structure of all other individuals in the subpopulation. This step is iterated N_t times to progressively update each brain graph in relation to other brain graphs using this graph-based diffusion process. Following N_t iterations, we produce the cluster-specific CBT by averaging (fusion) the diffused status matrices \mathbf{P}_i at the final iteration N_t :

$$\mathbf{CBT}_c = \frac{\sum_{i=1}^N n_c \mathbf{P}_i^{N_t}}{N_{n_c}}. \quad (5)$$

The update of $\mathbf{P}_i^{N_t}$ enables to iteratively integrate common and complementary information across brain networks during the fusion process.

(iii) LR CBT estimation. Ultimately, the CBT is computed by non-linearly fusing all cluster-specific CBTs using SNF (Wang et al., 2014a).

2.3. Proposed CBT-guided graph super-resolution

In the second stage, we define residual LR brain graphs which capture the deviation of each training LR subject from the estimated CBT. Then,

we learn multi-topology LR graph manifolds using graph topological measurements (e.g., degree, closeness, betweenness) by estimating residual LR similarity matrices modeling the relationship between pairs of training and testing LR graphs. Next, we non-linearly fuse these similarity matrices to predict HR brain graph from LR brain graph. Each of these steps is detailed as follows.

(i) Learning of multi-topology LR brain graph manifolds. In order to better capture the individual (i.e., subject-specific) traits, thereby producing a better representation of the subject on the population manifold, we create the residual graph by computing the absolute difference between each training LR graph and the estimated CBT. Therefore, the residual networks allow to model pairwise similarities between LR networks in relation to the average network (i.e., CBT). Next, we learn multi-topology LR graph manifolds using graph topological measures which nicely characterize both local and global relationships between brain ROIs. In particular, we use three topological measures including degree centrality, closeness centrality and betweenness centrality ([Liu et al., 2017a](#)). The degree centrality measures the number of edges connecting to a node (ROI). The degree centrality $D(n)$ of a node n is defined as:

$$D(n) = \sum_{n \neq j} x_{nj} \quad (6)$$

where $x_{nj} = 1$ if the connectivity of node n and node j exists; otherwise $x_{nj} = 0$.

The degree centrality defines the central nodes with the highest number of degree or connections by identifying the immediate neighbors of the node. So, in our case, it characterizes the *local* relationship between brain regions.

As for the closeness centrality $C(n)$, it quantifies the closeness between a node n and other nodes in a brain graph ([Beauchamp, 1965](#)):

$$C(n) = \frac{n_{r'} - 1}{\sum_{n \neq j} l_{nj}} \quad (7)$$

where $n_{r'}$ is the number of nodes and l_{nj} is the shortest path length between nodes n and j .

The closeness centrality of a node n is defined as the inverse of its shortest path lengths to all other nodes in the graph. It captures the effective outreach of a node via closest paths. Specifically, the node with the highest closeness will affect all other nodes with a short period of time (shortest path).

The betweenness centrality $B(n)$ defines the number of times a node i acts as a bridge along the shortest path between two other nodes in the graph (Liu et al., 2017a):

$$B(n) = \frac{2}{(n_{r'} - 1)(n_{r'} - 2)} \times \sum_{n \neq h \neq j} \frac{\xi_{hj}(n)}{\xi_{hj}} \quad (8)$$

where $\xi_{hj}(n)$ is the number of shortest paths between h and j that pass through node n , ξ_{hj} is the number of all shortest paths between h and j and $\frac{(n_{r'} - 1)(n_{r'} - 2)}{2}$ is the number of node pairs that do not include node n .

The betweenness centrality identifies nodes that mediate most information to all other nodes. Similarly to closeness centrality, betweenness centrality is based on the shortest path. They are widely used in the characterization of brain networks and allow to characterize the *global* relationship between brain regions and quantify their hubness (Fornito et al., 2016).

Hence, by using these centrality metrics, we can characterize each brain graph on both local and global levels (Fornito et al., 2016). Next, we learn for each topological measure a similarity matrix modeling the relationship between training and testing LR graphs using MKML (Wang et al., 2017). Last, we integrate the learned similarities of the three measures into a single similarity matrix using the non-linear similarity fusion technique introduced in (Wang et al., 2014a), which is ultimately used to identify the most similar training LR graphs to the testing LR graph for our prediction task.

(ii) Predicting high-resolution brain graph from low-resolution brain graph. Using leave-one-out cross-validation (LOO-CV) strategy, we identify for each left-out testing subject its K most similar LR training subjects. Last, by averaging the HR graphs of the K selected training subjects, we predict the testing HR brain graph in the target domain (Fig. 2–C).

3. Experimental results

Evaluation datasets and preprocessing pipeline. To evaluate our method, we used two functional connectomic datasets: the first one uses downsampling for generating LR brain graphs while the second one has both real LR and HR functional brain graphs.

Dataset 1 (downsampled HR (i.e., LR) and HR brain graphs). We evaluated our proposed framework on 505 subjects (266 ASD and 239 normal controls (NC)) from Autism Brain Imaging Data Exchange (ABIDE)

preprocessed public dataset ¹ using LOO-CV strategy (**Table 3**). Several preprocessing steps were implemented by the data processing assistant for resting-state fMRI (DPARSF) pipeline which is based on statistical parametric maps (SPM) and resting-state fMRI data analysis toolkit (REST). First, to ensure a steady signal, the first 10 volumes of rs-fMRI images were discarded. Based on a six-parameter (rigid body), all images were slice timing corrected and were realigned to the middle to cut down on inter-scan head motion (Tang et al., 2018). Then, the functional data were registered in montreal neurological institute (MNI) space with a resolution of $3 \times 3 \times 3 \text{ mm}^3$. To improve signal to noise ratio, spatial smoothing were then applied with a Gaussian kernel of 6 mm. Finally, band-pass filtering (0.01-0.1 Hz) was performed on the time series of each voxel (Price et al., 2014; Huang et al., 2017). These steps are detailed in this link: <http://preprocessed-connectomes-project.org/abide/>. Each brain rfMRI was partitioned into 116 ROIs.

Dataset 2 (real LR and HR brain graphs). We also evaluated our framework on 279 subjects from Southwest University Longitudinal Imaging Multimodal (SLIM) dataset², which includes brain and behavioral data across a long-term retest-duration within three and a half years, multimodal MRI scans provided a set of diffusion, structural and resting-state functional MRI images, along with rich samples of behavioral assessments addressed – cognitive, demographic and emotional information (Liu et al., 2017b). After several preprocessing steps for resting-state fMRI using Preprocessed Connectomes Project Quality Assessment Protocol³, each MRI is parcellated using two different atlases. The first one is the widely used Shen functional brain atlas where, for each subject, 268 regions of interest (ROIs) were generated (Shen et al., 2013). The second functional brain atlas is Dosenbach atlas which parcellates the brain into 160 anatomical regions, thereby producing functional brain graphs at 150×150 resolution (Dosenbach et al., 2010).

Parameter setting. For MKML parameters, we empirically set the number of clusters to $N_c = 2$, the number of nearest neighbors $k = 20$ and we used $n_k = 40$ kernels where each kernel is determined by a set of hyperparameters ($\sigma = \{1, \dots, 2\}$ with a step size of 0.25; number of top KNN neighbors in

¹<http://preprocessed-connectomes-project.org/abide/>

²http://fcon_1000.projects.nitrc.org/)

³(<http://preprocessed-connectomes-project.github.io/quality-assessment-protocol/>)

Table 2: ASD/NC data distribution.

Datasets	ASD/NC	
	ASD	NC
Number of subject	266	239
Male	173	122
Female	93	117
Mean age	17.64	17.31

$\{2, \dots, 16\}$) with a step of 2, where σ denotes the variance parameter of the Gaussian function. For SNF parameters, we also set the number of nearest neighbors to $q = 20$, the number of iterations $N_t = 20$ as recommended in (Wang et al., 2014a) for convergence. We fixed the number of closest LR neighbors to select for the target prediction task to $K = 25$ for a fair comparison across different methods. As for the number of nearest neighbors, we tuned them empirically for both SNF (Wang et al., 2014a) and MKML (Wang et al., 2017) (q and $k = \{10 : 10 : 100\}$). We note that the variation of the number of neighbors for both methods did not influence the performance of proposed and comparison methods. Hence, we opted for setting q and k to 20 which produced the best performance, although the improvement was negligible.

Evaluation and comparison methods. To evaluate the effectiveness of our proposed method (i.e., **BGSR**) in Fig. 2 for predicting HR from LR graphs generated using max and average pooling respectively, we carried out four major comparisons:

(1) **LR graphs + single MKML**: we used MKML for LR manifold learning using brain connectivity matrices (i.e., graph adjacency matrices) without using topological measurements or the CBT-derived residual graphs.

(2) **LR graphs + multiple MKML**: we computed the topological measurements of the LR brain graphs, then learned their similarity matrices without using the CBT and its derived residual graphs.

(3) **CBT + single MKML**: we used MKML for LR manifold learning of residual graphs without topological measurements (i.e., a single manifold is learned –not multiple).

(4) **netNorm** (Dhifallah et al., 2020): it is a novel framework that builds a connectional template for a population using a selective technique.

As illustrated in Fig. 2, we used the mean absolute error (MAE) and the Pearson correlation (PC) measures between the HR brain graphs and the predicted brain graph. The lower is the MAE the better is the per-

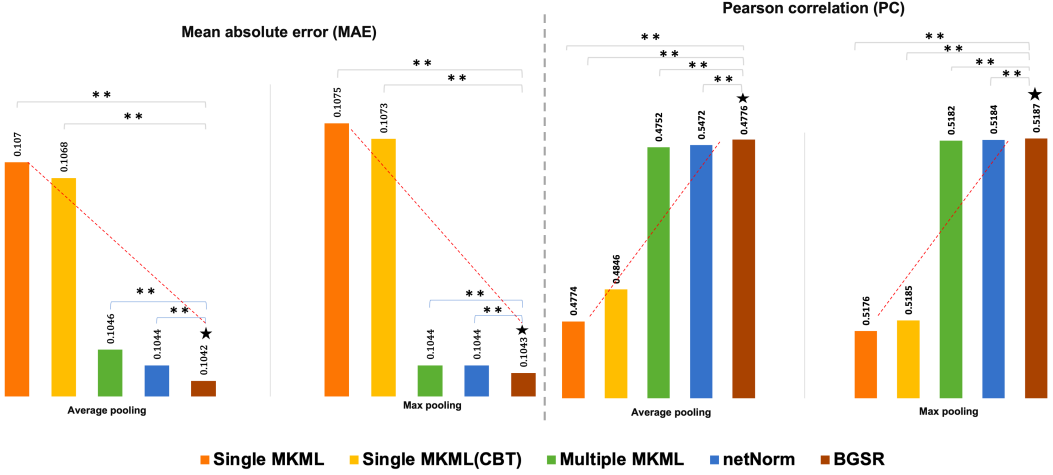


Figure 3: Brain graph super-resolution evaluation. Evaluating predicted HR brain graphs by our framework BGSR against four comparison methods (LR graphs + single MKML, LR graphs + multiple MKML, CBT + single MKML and netNorm ([Dhifallah et al., 2020](#))) using mean absolute error (MAE) and average Pearson correlation (PC) between ground truth and predicted HR graphs. MKML: multi-kernel manifold learning. CBT: connectional brain template. *: Our method (BGSR). (**): p-value < 0.05 using two-tailed paired t-test.

formance as opposed to PC where higher values correspond to a better LR super-resolution. Clearly, our BGSR consistently and significantly (p-value < 0.05 using two-tailed paired t-test) outperformed comparison methods in prediction HR brain graphs from LR graphs.

Topology-driven evaluation measures. To compare the topological structure of the predicted HR brain graphs with the ground truth graphs, we further computed the mean absolute error between the average degree, closeness and betweenness of the ground truth HR brain graphs and those of the predicted graphs, respectively. **Fig. 3** shows that our method consistently achieves the best topology-preserving predictions compared with its ablated versions as well as a state-of the-art method ([Dhifallah et al., 2020](#)) in CBT estimation using the proposed topology-based evaluation measures.

BGSR evaluation. We also evaluated our BGSR strategy on a real dataset 2 (**Fig. 5**). For both (MAE) and (PC), multiple MKML outperformed single MKML. Specifically, our proposed framework consistently achieved the best results with the smallest MAE and highest PC. Second, similar to **Fig. 3**, **Fig. 6** displays the MAE of the topological measures for each method

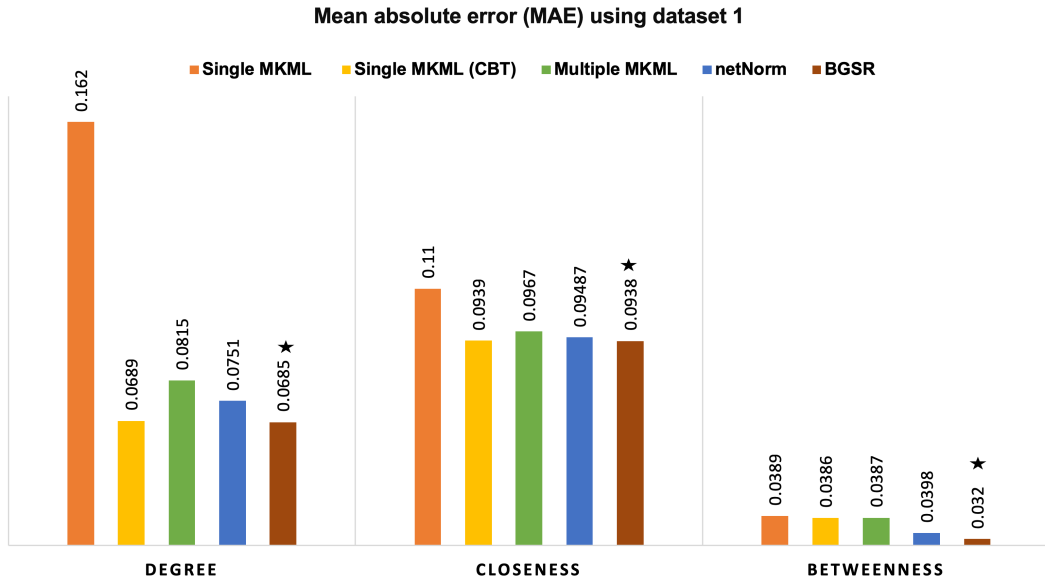


Figure 4: Evaluation of high-resolution brain graph synthesis by our framework BGSR against four comparison methods (LR graphs + single MKML, LR graphs + multiple MKML, CBT + single MKML and netNorm ([Dhifallah et al., 2020](#))) using three topological measures (degree, betweenness and closeness) and mean absolute error (MAE) between ground truth and predicted HR graphs in dataset 1. MKML: multi-kernel manifold learning. CBT: connectional brain template. *: Our method (BGSR).

to assess the prediction performance of the proposed method. Our method has a degree MAE of 0.263 which presents a significant improvement over comparison methods. Likewise, the lowest closeness and betweenness MAE were achieved by our method.

Evaluation of the discriminability of the predicted HR graphs using different feature selection methods. As a proof of concept of the discriminative power of the predicted HR brain graphs, we compared the performance of a linear classifier combined with two different feature selection methods, respectively, which we trained using LR and predicted HR graphs by different strategies to distinguish between ASD and NC functional brain graphs:

(1) A linear support vector machine (SVM) combined with infinite feature selection (IFS)⁴ method which outperformed 8 feature selection methods 8 (SVM-REF (Guyon et al., 2002), MutInf (Zaffalon and Hutter, 2002), Relief-F (Liu et al., 2017a), FSV (Grinblat et al., 2010), Fisher (Gu et al., 2012), Ens.SVM-RFE (Gu et al., 2012), SW SVM-RFE (Yu et al., 2012), SW Relief-F (Yu et al., 2012)) using 13 datasets (USPS, GINA, Gisette, Colon, Lymphoma, Leukemia, Lung181, DLBCL, MADELON, Caltech-101, Caltech256, VOC2007, VOC2012).

(2) Network atlas-guided feature selection (NAGFS)⁵ (Mhiri and Rekik, 2020) which is a fast and accurate feature selection method tailored for graph-based datasets.

As shown in **Fig. 8** the predicted HR from LR functional brain graphs boosted the classification results for autistic subjects by 14.33% using SVM+IFS method and 16.48% using NAGFS method compared with LR functional graphs.

On top of that, our method can be used to reconstruct HR graphs in a very low computational time (0.086 seconds per subject on average) compared to the typically used FreeSurfer/SPM image processing pipelines (of the order of hours). Hence, our method can scale well in both memory and run time for larger graphs.

⁴<https://uk.mathworks.com/matlabcentral/fileexchange/54763-infinite-feature-selection>

⁵<https://github.com/basirala/NAGFS-PY>

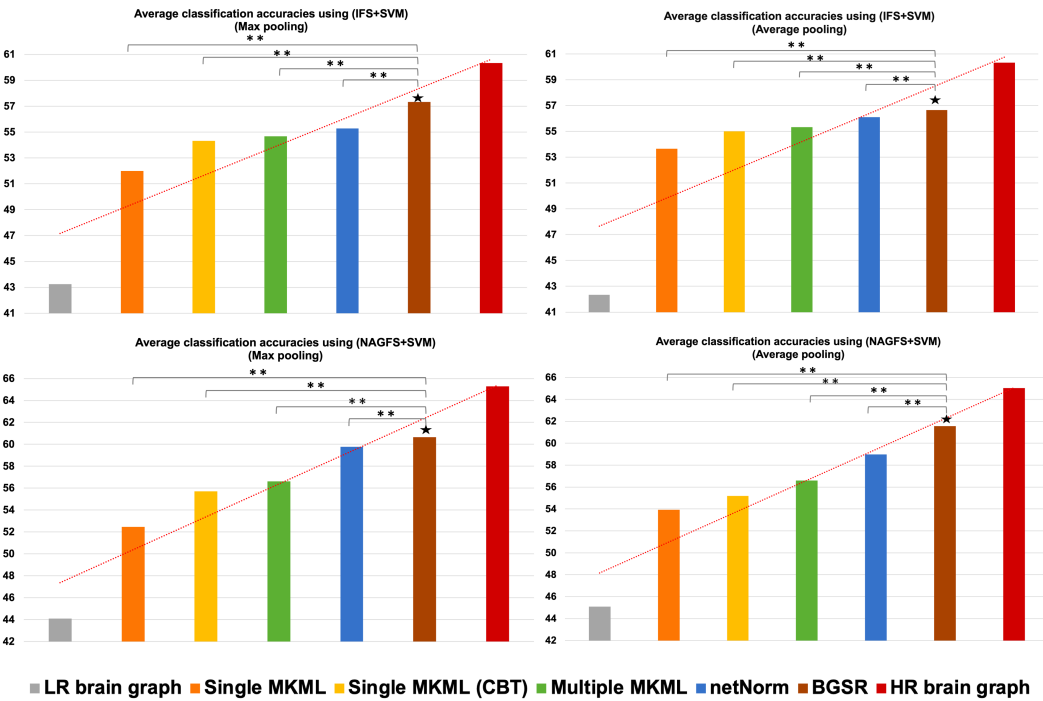


Figure 5: ASD/NC classification using different brain graphs derived from dataset 1. Average classification accuracies by (SVM+IFS) (Roffo et al., 2015) and (SVM+NAGFS) (Mhiri and Rekik, 2020) classification models using LR graphs generated by max/average pooling downsampling strategies, ground truth HR graphs (red bars), predicted HR graphs by comparison methods, and predicted HR graph by our BGSR method and comparison methods. *: Our method (BGSR). (**): p-value < 0.05 using two-tailed paired t-test.

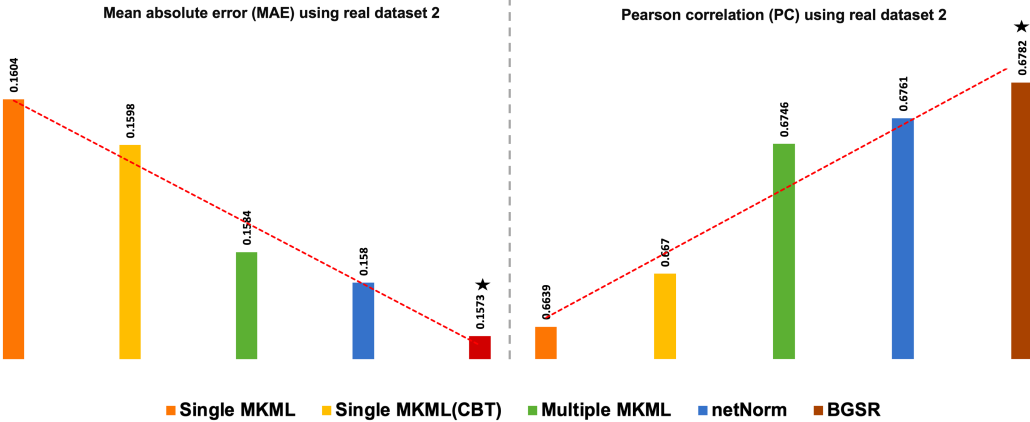


Figure 6: High-resolution (HR) brain graph prediction evaluation using real dataset 2. Evaluating prediction performance by our framework BGSR against four comparison methods (LR graphs + single MKML, LR graphs + multiple MKML, CBT + single MKML and netNorm ([Dhifallah et al., 2020](#))) using mean absolute error (MAE) and average Pearson correlation (PC) between ground truth and predicted HR graphs. MKML: multi-kernel manifold learning. CBT: connectional brain template. \star : Our method (BGSR).

4. Discussion

Brain graph super-resolution is an untapped research field that cross-pollinates graph theory and data super-resolution. In this paper, we introduced a novel learning-based technique to super-resolve undirected fully connected graphs with application to functional brain connectomes with the aim of boosting the diagnosis of autism spectrum disorder (ASD). Our learning-based framework comprises three steps. *First*, we learn how to estimate a centered and representative connectional brain template which would help better capture the individuality of each LR brain graph via the estimated residual graph. *Second*, we propose a simple but effective strategy to predict HR brain graphs from LR graphs rooted in the estimated LR CBT. Our approach has three compelling strengths: (1) The use of the estimated CBT significantly boosted the prediction of HR graphs in comparison with its variants and state-of-the art methods, (2) the learning of different manifolds where multi-topology residual LR graphs are nested significantly improved the quality of the super-resolved graphs, and (3) our method consistently outperformed comparison methods using several evaluation measures for two different large-scale datasets.

Insights into baseline methods. As shown in Fig. 2, (LR graphs + sin-

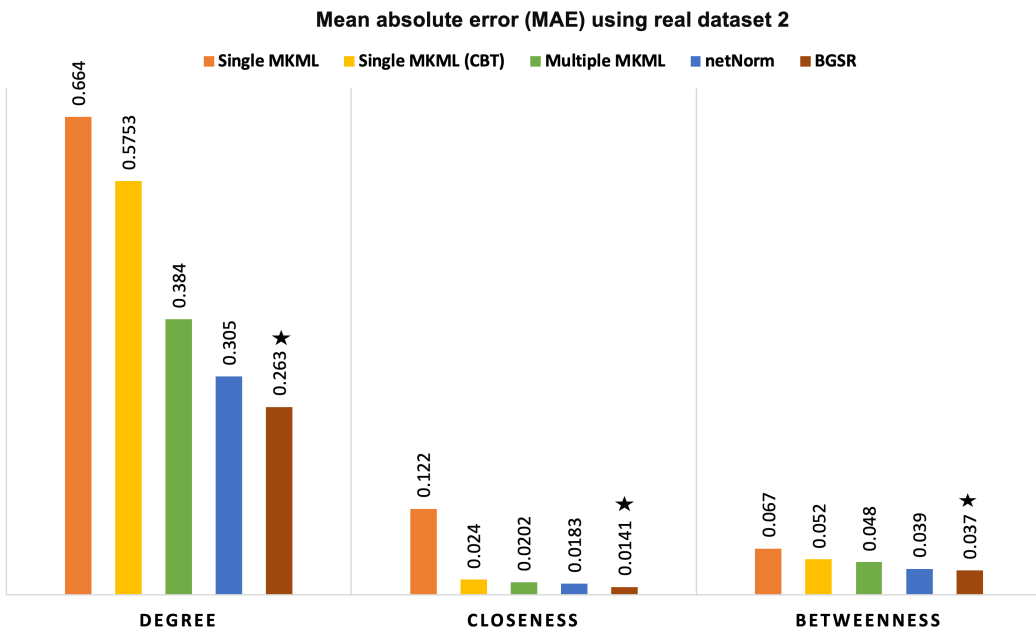


Figure 7: Evaluating HR graph prediction performance by our framework BGSR against four comparison methods (LR graphs + single MKML, LR graphs + multiple MKML, CBT + single MKML and netNorm ([Dhifallah et al., 2020](#))) using three topological measures (degree, betweenness and closeness) and mean absolute error (MAE) between ground truth and predicted HR graphs using real dataset 2. MKML: multi-kernel manifold learning. CBT: connectional brain template. *: Our method.

Table 3: Mean Frobenius distance between the estimated connectional brain template and all individual networks in the population while varying the number of clusters.

Number of clusters	Frobenius distance
1 (without clustering)	1.53
2	0.62
3	0.64
4	0.65
5	0.68
6	0.71

gle MKML) produced the highest mean absolute error between ground truth and predicted HR graph, followed by (CBT + single MKML) using both max pooling and average pooling. These results can be explained by the fact that learning of a single manifold based solely on graph connectivity strengths is not sufficient to fully capture the inherent graph data distribution as this overlooks important graph properties such as topology and structure. For this reason, we proposed to learn multi-topology LR graph manifolds (i.e., multiple MKML) using graph topological measurements which characterize both local and global relationships between brain ROIs in each graph. Moreover, netNorm framework (Dhifallah et al., 2020), which was mainly designed for CBT estimation, overlooks data heterogeneity. This might explain why netNorm has lower HR prediction and classification results than our BGSR. Notably, BGSR consistently and significantly outperformed other variants as well as a state-of-the art method in both max pooling and average pooling. Similarly, Pearson correlation between ground truth and predicted HR graph showed that our method achieved the graph super-resolution results. This demonstrates that the learned CBT well captures the individuality of each subject via the estimated residual graph, which produced a better multi-topology manifold learning compared with methods without CBT, thereby boosting graph super-resolution and supporting our hypothesis (**Fig. 1**).

Fig. 4 displays the LR, HR, and predicted HR graphs by BGSR and the three comparison methods (LR graphs + single MKML, CBT + single MKML, and LR graphs + multiple MKML) for two representative subjects. For each subject, we display LR brain graph and ground truth on the left, prediction in the middle and the prediction residual on the right. The prediction residual graph is produced by taking the absolute difference between the ground truth and predicted HR graph. An average value of the residual matrix is displayed on top of each prediction residual graph. We observe that the residual was noticeably reduced by our BGSR method.

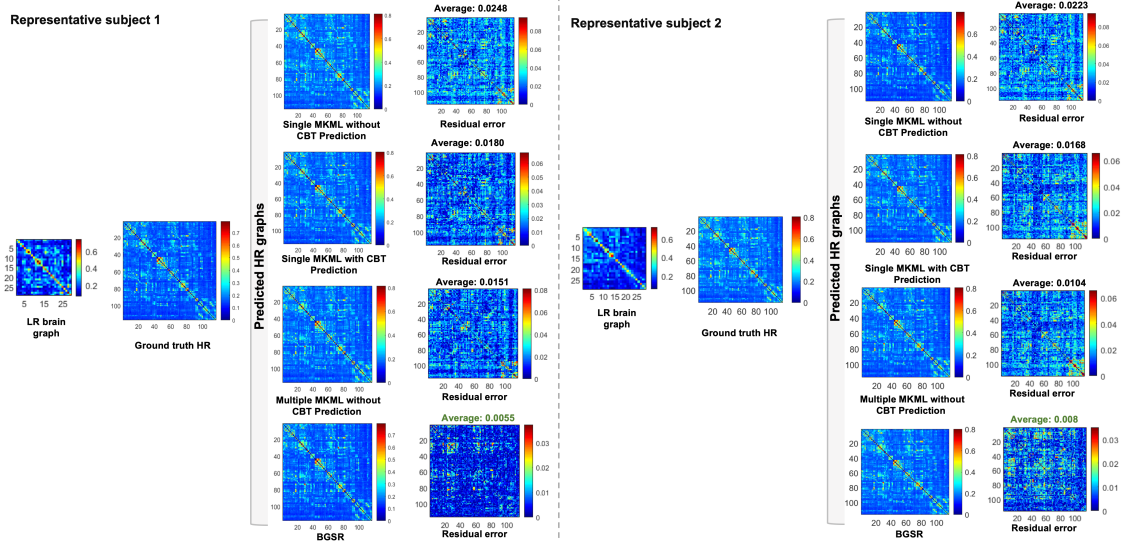


Figure 8: Comparison between the ground truth and predicted HR graphs by BGSR and three baseline methods (LR graphs + single MKML, LR graphs + multiple MKML, and CBT + single MKML method) using two representative subjects from dataset 1. We display the residual matrices computed using the absolute difference between ground truth and predicted brain graphs.

As shown in **Table 3**, we computed the mean Frobenius distance between the estimated CBT and all individual networks in the population using different numbers of clusters. A smaller distance indicates a more centered CBT with respect to all individuals in the population and all views. We found that $N_c = 2$ achieves the best results.

On top of that, devising a fast and efficient graph super-resolution technique with low computationally cost that can meet the formidable challenge of exploding large datasets remains a nascent area of research. In this study, we show that our method can be used to reconstruct HR graphs in a low computational time.

Discriminability of the superresolved brain graphs. To further demonstrate the diagnostic potential of our prediction framework, we compared the performance of a linear classifier combined with two feature selection methods, respectively, which we trained using LR and predicted HR graphs by different strategies to distinguish between ASD and NC graphs: (1) A linear support vector machine (SVM) combined with infinite feature selection (IFS) method (Roffo et al., 2015), and (2) Network atlas-guided feature selection (NAGFS) (Mhiri and Rekik, 2020), which is a fast and accurate feature selection method. **Fig. 8** displays the average classification accuracies by SVM+IFS method and NAGFS methods. We report the average accuracy across different numbers of selected features: $f_n = \{90, \dots, 150\}$ with a step size of 20. Notably, the predicted HR from LR functional brain graphs boosted classification results for ASD subjects by 14.33% for SVM+IFS method and 16.48% for NAGFS method compared with LR functional graphs synthesized using average pooling. This demonstrates that the *predicted* HR graphs by our method have the potential to largely boost the diagnosis of neurological disorders in comparison with using LR data.

Insights into topological measures. To investigate the fidelity of the predicted HR graphs to the original HR graphs in topology and structure, we further evaluated our framework using different topological metrics (degree, closeness and betweenness). As shown in **Fig. 3** and **Fig. 6**, our method produced the smallest MAE between ground truth and predicted HR graphs for all topological measurements. This might indicate that the most important nodes within a brain graph are the same for both ground truth and predicted HR. Therefore, the results demonstrate the effectiveness of our prediction framework.

Insights into the real data results. To further demonstrate the utility of the proposed method, we conducted experiments on a real connectomic

dataset with both real LR and HR graphs derived from two different brain parcellations. From [Fig. 5](#) and [Fig. 6](#), we can make the following observations:

First, in terms of the mean absolute error (MAE) values, BGSR achieved the lowest prediction error across all baseline methods.

Second, the proposed method consistently outperformed other methods in terms of Pearson correlation (PC) between ground truth and predicted HR graphs.

Third, to ensure the reliability of BGSR in generating topologically sound brain graphs at high resolution, we evaluated the performance of our framework by computing the mean absolute error between the degree, closeness and betweenness of the HR brain graphs and those of the predicted brain graphs. Our method clearly produces the best graph super-resolution results.

We can conclusively confirm that the proposed brain graph super-resolution framework performs equally well for both synthetic and real datasets.

Node-invariance. An appealing aspect of our BGSR method is that it is node-invariant. Indeed, our method is based on selecting the best training samples for the target prediction task using similarity metric learning between pairs of residual graph representations that we designed. This ‘residual’ manifold learning is based on the topological measures of the residual networks which is invariant to the order in which we arrange ROIs (nodes) in the brain connectivity (adjacency) matrix. Graph statistics such as centrality measures are invariant to the node ordering in the graph (or adjacency matrix). Our synthetic experiment using ABIDE dataset further supports this observation as we synthesize fake ROIs in the LR domain by max-pooling and average-pooling.

Neuro-biomarkers. [Fig. 9](#), displays the top 5 most discriminative functional connectivities identified from our predicted HR brain graph. We notice that most discriminative functional brain connectivities belong to the frontal lobe. Moreover, we identified other discriminative connectivities between different regions such as amygdala (temporal lobe), cerebellum which were reported in previous works ([Chaddad et al., 2017](#); [Zalla and Sperduti, 2013](#); [Amaral et al., 2003](#)). The frontal lobe has an important role in forming memories ([Curran et al., 1997](#)), speech and language production ([Alexander et al., 1989](#)), making decisions ([Collins and Koechlin, 2012](#)) and understanding and reacting to others which might explain the prevalence of altered brain connectivities in this brain labor region. Additionally, ([Becker and Stoodley, 2013](#)) mentioned that the cerebellum has emerged as one of the key brain re-

gions affected in autism that different parts of the cerebellum have a reduced size than NC patients. Furthermore, (Kleinhans et al., 2010) showed that the abnormal facial expressions of the ASD patients are thought to be associated with amygdala abnormalities. Also, during memory retrieval, the ASD group exhibited attenuated lateral frontal activity and substantially reduced hippocampal connectivity (Cooper et al., 2017). (Kim et al., 2010; Adolphs, 2001) demonstrated that the mediate impairments of social behaviors are caused by the abnormalities in the frontal lobe, superior temporal cortex and parietal cortex. All these studies support the discriminative functional connectivities revealed by our predicted HR brain graph.

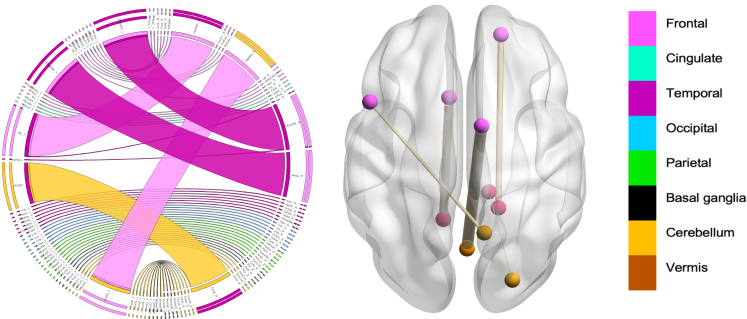


Figure 9: The strongest connections present the 5 most discriminative functional brain connections between ASD and NC groups. The circular graphs were generated using Circos table viewer (Krzywinski et al., 2009). We used Brain Net Viewer Software (Xia et al., 2013) to display the regions of interest involving the most discriminative connectivities.

Limitations and future directions. Although our proposed method achieved excellent results, there are several improvements that can be explored in our future work.

Using other downsampling techniques. In this work, we have synthesized LR brain networks using only max-pooling and average pooling. However, one can alternatively use more sophisticated graph downsampling techniques such as interpolation-based methods (Chevalier and Safro, 2009), V-cycle method (Buluç et al., 2016), grouping-based methods, bit compression-based methods and influence-based methods (Liu et al., 2018).

Using other brain graph representations. As yet, our method was evaluated using only functional brain graphs derived from rfMRI. We aim to use our method to super-resolve other types of brain graphs including structural brain networks estimated from diffusion MRI (Bullmore and Sporns, 2009)

and morphological brain networks estimated from conventional T1- weighted MRI (Morris and Rekik, 2017; Soussia and Rekik, 2017; Mahjoub et al., 2018; Zhu and Rekik, 2018; Nebli and Rekik, 2019).

Using other topological measures. So far, we have only used centrality measures to learn the data residual manifold for the target brain graph super-resolution. As such, we are clearly enforcing the reconstruction of HR graphs somehow preserving centrality (i.e., hubs), which in turn, overlooks other important characteristic of the graph that centrality by itself does not provide, most noticeably segregation. In our future work, we intend to integrate other topological measures such as graph clustering coefficient which can better capture HR brain network segregation (Bullmore and Sporns, 2012; Rudie et al., 2013).

Using other graph representation learning. In our work, we mainly relied on graph topological measures to model the similarity between brain graphs. Alternatively, one can also leverage recent deep graph representation learning frameworks (Hamilton et al., 2017) such as graph autoencoders to automatically learn the similarity between pairs of graphs instead of handcrafting it.

Handling multi-resolution brain graphs. The proposed method can only predict a single higher resolution graph from a low-resolution graph. It would be interesting to generalize it to multi-resolution graph prediction from a source graph. In other words, one can jointly learn how to synthesize brain graphs at multiple resolutions from a single source graph.

Strong assumption about sample similarity consistency across domains. Assuming that the similarity between samples in the source domain will be preserved in the target domain using sample-to-sample or residual-to-residual similarity learning (**Fig. 1**) is a strong assumption that should be relaxed when the target or source domains has noisy observations or outliers.

5. Conclusion

In this paper, we design the first brain graph super-resolution using functional brain data with the aim to boost neurological disorder diagnosis. Our framework learns HR graphs without resorting to the computationally expensive image processing pipelines for connectome construction at high-resolution scales. The proposed BGSR method achieved the best prediction performance in comparison with baseline methods, and remarkably boosted the classification accuracy using predicted HR graphs in comparison to LR

graphs. So far, we have only evaluated the proposed method on functional brain graphs for a particular neurological disorder (i.e., autism spectrum disorder). In our future work, we will evaluate our framework on larger connectomic datasets covering a diverse range of neurological disorders such as brain dementia. Furthermore, we will extend our work to handle brain graphs derived from several MRI modalities to learn how to jointly super-resolve multimodal brain graphs sharing connectional traits.

6. Acknowledgements

This project has been funded by the 2232 International Fellowship for Outstanding Researchers Program of TUBITAK (Project No:118C288) supporting I. Rekik. However, all scientific contributions made in this project are owned and approved solely by the authors. More information about the project can be found at <https://basira-lab.com/reprime/>.

- Adolphs, R., 2001. The neurobiology of social cognition. *Current opinion in neurobiology* 11, 231–239.
- Alexander, M.P., Benson, D.F., Stuss, D.T., 1989. Frontal lobes and language. *Brain and language* 37, 656–691.
- Amaral, D.G., Corbett, B.A., et al., 2003. The amygdala, autism and anxiety. *Novartis Found Symp* 251, 87.
- Ashburner, J., 2012. SPM: a history. *Neuroimage* 62, 791–800.
- Bahrami, K., Rekik, I., Shi, F., Shen, D., 2017a. Joint reconstruction and segmentation of 7t-like mr images from 3t mri based on cascaded convolutional neural networks. *International Conference on Medical Image Computing and Computer-Assisted Intervention*, 764–772.
- Bahrami, K., Shi, F., Rekik, I., Gao, Y., Shen, D., 2017b. 7t-guided super-resolution of 3t MRI. *Medical physics* 44, 1661–1677.
- Bahrami, K., Shi, F., Rekik, I., Shen, D., 2016. Convolutional neural network for reconstruction of 7t-like images from 3t mri using appearance and anatomical features. *Deep Learning and Data Labeling for Medical Applications*, 39–47.
- Bassett, D.S., Khambhati, A.N., Grafton, S.T., 2017. Emerging frontiers of neuroengineering: a network science of brain connectivity. *Annual review of biomedical engineering* 19, 327–352.
- Bastiani, M., Andersson, J.L., Cordero-Grande, L., Murgasova, M., Hutter, J., Price, A.N., Makropoulos, A., Fitzgibbon, S.P., Hughes, E., Rueckert, D., et al., 2019. Automated processing pipeline for neonatal diffusion mri in the developing human connectome project. *NeuroImage* 185, 750–763.
- Beauchamp, M.A., 1965. An improved index of centrality. *Behavioral science* 10, 161–163.
- Becker, E.B., Stoodley, C.J., 2013. Autism spectrum disorder and the cerebellum 113, 1–34.
- Bellec, P., Benhajali, Y., Carbonell, F., Dansereau, C., Albouy, G., Pelland, M., Craddock, C., Collignon, O., Doyon, J., Stip, E., et al., 2015. Impact

- of the resolution of brain parcels on connectome-wide association studies in fMRI. *Neuroimage* 123, 212–228.
- Bessadok, A., Mahjoub, M.A., Rekik, I., 2019. Symmetric dual adversarial connectomic domain alignment for predicting isomorphic brain graph from a baseline graph. International Conference on Medical Image Computing and Computer-Assisted Intervention , 465–474.
- Bullmore, E., Sporns, O., 2009. Complex brain networks: graph theoretical analysis of structural and functional systems. *Nature reviews neuroscience* 10, 186.
- Bullmore, E., Sporns, O., 2012. The economy of brain network organization. *Nature Reviews Neuroscience* 13, 336–349.
- Buluç, A., Meyerhenke, H., Safro, I., Sanders, P., Schulz, C., 2016. Recent advances in graph partitioning , 117–158.
- Bunke, H., Riesen, K., 2011. Recent advances in graph-based pattern recognition with applications in document analysis. *Pattern Recognition* 44, 1057–1067.
- Chaddad, A., Desrosiers, C., Hassan, L., Tanougast, C., 2017. Hippocampus and amygdala radiomic biomarkers for the study of autism spectrum disorder. *BMC neuroscience* 18, 52.
- Chen, S., Sandryhaila, A., Moura, J.M., Kovacevic, J., 2014. Signal denoising on graphs via graph filtering , 872–876.
- Chen, X., Pan, L., 2018. A survey of graph cuts/graph search based medical image segmentation. *IEEE reviews in biomedical engineering* 11, 112–124.
- Chevalier, C., Safro, I., 2009. Comparison of coarsening schemes for multi-level graph partitioning , 191–205.
- Collins, A., Koechlin, E., 2012. Reasoning, learning, and creativity: frontal lobe function and human decision-making. *PLoS biology* 10, e1001293.
- Cooper, R.A., Richter, F.R., Bays, P.M., Plaisted-Grant, K.C., Baron-Cohen, S., Simons, J.S., 2017. Reduced hippocampal functional connectivity during episodic memory retrieval in autism. *Cerebral Cortex* 27, 888–902.

- Curran, T., Schacter, D.L., Norman, K.A., Galluccio, L., 1997. False recognition after a right frontal lobe infarction: Memory for general and specific information. *Neuropsychologia* 35, 1035–1049.
- Dhifallah, S., Rekik, I., Initiative, A.D.N., et al., 2020. Estimation of connectional brain templates using selective multi-view network normalization. *Medical Image Analysis* 59, 101567.
- Dosenbach, N.U., Nardos, B., Cohen, A.L., Fair, D.A., Power, J.D., Church, J.A., Nelson, S.M., Wig, G.S., Vogel, A.C., Lessov-Schlaggar, C.N., et al., 2010. Prediction of individual brain maturity using fmri. *Science* 329, 1358–1361.
- Ezzine, B.E., Rekik, I., 2019. Learning-guided infinite network atlas selection for predicting longitudinal brain network evolution from a single observation. *International Conference on Medical Image Computing and Computer-Assisted Intervention* , 796–805.
- Fornito, A., Zalesky, A., Bullmore, E., 2016. Fundamentals of brain network analysis .
- Freeman, L.C., 1978. Centrality in social networks conceptual clarification. *Social networks* 1, 215–239.
- Glasser, M.F., Coalson, T.S., Robinson, E.C., Hacker, C.D., Harwell, J., Yacoub, E., Ugurbil, K., Andersson, J., Beckmann, C.F., Jenkinson, M., et al., 2016. A multi-modal parcellation of human cerebral cortex. *Nature* 536, 171.
- Goyal, P., Ferrara, E., 2018. Graph embedding techniques, applications, and performance: A survey. *Knowledge-Based Systems* 151, 78–94.
- Grinblat, G.L., Izetta, J., Granitto, P.M., 2010. Svm based feature selection: Why are we using the dual? , 413–422.
- Gu, Q., Li, Z., Han, J., 2012. Generalized fisher score for feature selection. *arXiv preprint arXiv:1202.3725* .
- Guyon, I., Weston, J., Barnhill, S., Vapnik, V., 2002. Gene selection for cancer classification using support vector machines. *Machine learning* 46, 389–422.

- Hamilton, W.L., Ying, R., Leskovec, J., 2017. Representation learning on graphs: Methods and applications. arXiv preprint arXiv:1709.05584 .
- Hegeman, T., Iosup, A., 2018. Survey of graph analysis applications. arXiv preprint arXiv:1807.00382 .
- Huang, X., Huang, C., 2018. Ngd: Filtering graphs for visual analysis. IEEE Transactions on Big Data 4, 381–395.
- Huang, X.H., Song, Y.Q., Liao, D.A., Lu, H., 2017. Detecting community structure based on optimized modularity by genetic algorithm in resting-state fMRI , 457–464.
- Joyce, K.E., Laurienti, P.J., Burdette, J.H., Hayasaka, S., 2010. A new measure of centrality for brain networks. PloS one 5, e12200.
- Kim, J.E., Lyoo, I.K., Estes, A.M., Renshaw, P.F., Shaw, D.W., Friedman, S.D., Kim, D.J., Yoon, S.J., Hwang, J., Dager, S.R., 2010. Laterobasal amygdalar enlargement in 6-to 7-year-old children with autism spectrum disorder. Archives of general psychiatry 67, 1187–1197.
- Kleinhans, N.M., Richards, T., Weaver, K., Johnson, L.C., Greenson, J., Dawson, G., Aylward, E., 2010. Association between amygdala response to emotional faces and social anxiety in autism spectrum disorders. Neuropsychologia 48, 3665–3670.
- Kruschwitz, J., List, D., Waller, L., Rubinov, M., Walter, H., 2015. Graph-Var: a user-friendly toolbox for comprehensive graph analyses of functional brain connectivity. Journal of neuroscience methods 245, 107–115.
- Krzywinski, M.I., Schein, J.E., Birol, I., Connors, J., Gascoyne, R., Horsman, D., Jones, S.J., Marra, M.A., 2009. Circos: An information aesthetic for comparative genomics. Genome Research <http://genome.cshlp.org/content/early/2009/06/15/gr.092759.109.full.pdf+html>.
- Li, W., Andreasen, N.C., Nopoulos, P., Magnotta, V.A., 2013. Automated parcellation of the brain surface generated from magnetic resonance images. Frontiers in neuroinformatics 7, 23.
- Liu, J., Li, M., Pan, Y., Lan, W., Zheng, R., Wu, F.X., Wang, J., 2017a. Complex brain network analysis and its applications to brain disorders: a survey. Complexity 2017.

- Liu, W., Wei, D., Chen, Q., Yang, W., Meng, J., Wu, G., Bi, T., Zhang, Q., Zuo, X.N., Qiu, J., 2017b. Longitudinal test-retest neuroimaging data from healthy young adults in southwest china. *Scientific data* 4, 170017.
- Liu, Y., Safavi, T., Dighe, A., Koutra, D., 2018. Graph summarization methods and applications: A survey. *ACM Computing Surveys (CSUR)* 51, 1–34.
- Mahjoub, I., Mahjoub, M.A., Rekik, I., 2018. Brain multiplexes reveal morphological connectional biomarkers fingerprinting late brain dementia states. *Scientific reports* 8, 4103.
- Makropoulos, A., Robinson, E.C., Schuh, A., Wright, R., Fitzgibbon, S., Bozek, J., Counsell, S.J., Steinweg, J., Vecchiato, K., Passerat-Palmbach, J., et al., 2018. The developing human connectome project: a minimal processing pipeline for neonatal cortical surface reconstruction. *Neuroimage* 173, 88–112.
- Mhiri, I., Rekik, I., 2020. Joint functional brain network atlas estimation and feature selection for neurological disorder diagnosis with application to autism. *Medical image analysis* 60, 101596.
- Mijalkov, M., Kakaei, E., Pereira, J.B., Westman, E., Volpe, G., Initiative, A.D.N., et al., 2017. Braph: a graph theory software for the analysis of brain connectivity. *PloS one* 12.
- Morris, C., Rekik, I., 2017. Autism spectrum disorder diagnosis using sparse graph embedding of morphological brain networks. *Graphs in Biomedical Image Analysis, Computational Anatomy and Imaging Genetics* , 12–20.
- Nebli, A., Rekik, I., 2019. Gender differences in cortical morphological networks. *Brain imaging and behavior* , 1–9.
- Oxtoby, N.P., Garbarino, S., Firth, N.C., Warren, J.D., Schott, J.M., Alexander, D.C., Initiative, A.D.N., et al., 2017. Data-driven sequence of changes to anatomical brain connectivity in sporadic alzheimer’s disease. *Frontiers in neurology* 8, 580.
- Park, S.C., Park, M.K., Kang, M.G., 2003. Super-resolution image reconstruction: a technical overview. *IEEE signal processing magazine* 20, 21–36.

- Price, T., Wee, C.Y., Gao, W., Shen, D., 2014. Multiple-network classification of childhood autism using functional connectivity dynamics , 177–184.
- Rekik, I., Li, G., Lin, W., Shen, D., 2015. Prediction of longitudinal development of infant cortical surface shape using a 4d current-based learning framework. International Conference on Information Processing in Medical Imaging , 576–587.
- Rekik, I., Li, G., Lin, W., Shen, D., 2016. Predicting infant cortical surface development using a 4D varifold-based learning framework and local topography-based shape morphing. Medical image analysis 28, 1–12.
- Rekik, I., Li, G., Lin, W., Shen, D., 2017. Estimation of brain network atlases using diffusive-shrinking graphs: Application to developing brains. International Conference on Information Processing in Medical Imaging , 385–397.
- Roffo, G., Melzi, S., Cristani, M., 2015. Infinite feature selection. Proceedings of the IEEE International Conference on Computer Vision , 4202–4210.
- Rudie, J.D., Brown, J., Beck-Pancer, D., Hernandez, L., Dennis, E., Thompson, P., Bookheimer, S., Dapretto, M., 2013. Altered functional and structural brain network organization in autism. NeuroImage: clinical 2, 79–94.
- Rueda, A., Malpica, N., Romero, E., 2013. Single-image super-resolution of brain mr images using overcomplete dictionaries. Medical image analysis 17, 113–132.
- Shen, X., Tokoglu, F., Papademetris, X., Constable, R.T., 2013. Groupwise whole-brain parcellation from resting-state fmri data for network node identification. Neuroimage 82, 403–415.
- Shen, Y., Traganitis, P.A., Giannakis, G.B., 2017. Nonlinear dimensionality reduction on graphs , 1–5.
- Soussia, M., Rekik, I., 2017. High-order connectomic manifold learning for autistic brain state identification. International Workshop on Connectomics in Neuroimaging , 51–59.
- Tang, C., Wei, Y., Zhao, J., Nie, J., 2018. The dynamic measurements of regional brain activity for resting-state fMRI: d-alff, d-falff and d-reho , 190–197.

- Tian, J., Ma, K.K., 2011. A survey on super-resolution imaging. *Signal, Image and Video Processing* 5, 329–342.
- Von Luxburg, U., 2007. A tutorial on spectral clustering. *Statistics and computing* 17, 395–416.
- Wang, B., Mezlini, A.M., Demir, F., Fiume, M., Tu, Z., Brudno, M., Haibe-Kains, B., Goldenberg, A., 2014a. Similarity network fusion for aggregating data types on a genomic scale. *Nature methods* 11, 333.
- Wang, B., Ramazzotti, D., De Sano, L., Zhu, J., Pierson, E., Batzoglou, S., 2018. SIMLR: A Tool for Large-Scale Genomic Analyses by Multi-Kernel Learning. *Proteomics* 18, 1700232.
- Wang, B., Zhu, J., Pierson, E., Ramazzotti, D., Batzoglou, S., 2017. Visualization and analysis of single-cell rna-seq data by kernel-based similarity learning. *Nature methods* 14, 414.
- Wang, Y.H., Qiao, J., Li, J.B., Fu, P., Chu, S.C., Roddick, J.F., 2014b. Sparse representation-based MRI super-resolution reconstruction. *Measurement* 47, 946–953.
- Xia, M., Wang, J., He, Y., 2013. Brainnet viewer: a network visualization tool for human brain connectomics. *PloS one* 8, e68910.
- Xiao, B., Cheng, J., Hancock, E.R., 2013. Graph-based methods in computer vision: developments and applications .
- Yan, S., Xu, D., Zhang, B., Zhang, H.J., Yang, Q., Lin, S., 2007. Graph embedding and extensions: A general framework for dimensionality reduction. *IEEE Transactions on Pattern Analysis & Machine Intelligence* , 40–51.
- Yu, L., Han, Y., Berens, M.E., 2012. Stable gene selection from microarray data via sample weighting. *IEEE/ACM Transactions on Computational Biology and Bioinformatics* 9, 262–272.
- Zaffalon, M., Hutter, M., 2002. Robust feature selection using distributions of mutual information. *Proceedings of the 18th International Conference on Uncertainty in Artificial Intelligence (UAI-2002)* , 577–584.

Zalla, T., Sperduti, M., 2013. The amygdala and the relevance detection theory of autism: an evolutionary perspective. *Frontiers in human neuroscience* 7, 894.

Zhu, M., Rekik, I., 2018. Multi-view brain network prediction from a source view using sample selection via cca-based multi-kernel connectomic manifold learning. *International Workshop on Predictive Intelligence In MEDicine* , 94–102.